Available online at www.sciencedirect.com
ScienceDirect
Journal of Theoretical Biology 249 (2007) 723–736
Journal of Theoretical Biology
www.elsevier.com/locate/yjtbi

A stochastic analysis of actin polymerization in the presence of twinfilin and gelsolin ☆

Anastasios Matzavinos[a,*], Hans G. Othmer[a,b]

[a]School of Mathematics, University of Minnesota, Minneapolis, MN 55455, USA
[b]Digital Technology Center, University of Minnesota, Minneapolis, MN 55455, USA

Received 8 March 2007; received in revised form 2 August 2007; accepted 16 August 2007
Available online 28 August 2007

Abstract

We develop an efficient stochastic simulation algorithm for analyzing actin filament growth and decay in the presence of various actin-binding proteins. The evolution of nucleotide profiles of filaments can be tracked and the resulting feedback to actin-binding proteins is incorporated. The computational efficiency of the new method enables us to focus on experimentally realistic problems, and as one example we use it to analyze the experimental data of Helfer et al. [(2006). Mammalian twinfilin sequesters ADP-G-actin and caps filament barbed ends: implications in motility. EMBO J. 25, 1184–1195] on the capping and G-actin sequestering activity of twinfilin. We show that the binding specificity of twinfilin for ADP-G-actin is crucial for the observed biphasic evolution of the filament length distribution in the presence of twinfilin, and we demonstrate that twinfilin can be an essential part of the molecular machinery for regulating filament lengths after a short burst of polymerization. Significantly, our simulations indicate that the pyrenyl-actin fluorescence experiments would fail to report the emergence of large filaments under certain experimental conditions.

Keywords: Stochastic simulation algorithm; Polymerization; Actin; Gelsolin; Twinfilin; Capping protein

1. Introduction

1.1. Sequestration and capping activities of mammalian twinfilin

Two recent papers on twinfilins have highlighted the importance of these proteins for the regulation of actin dynamics. Helfer et al. (2006) demonstrated experimentally that twinfilins sequester ADP-G-actin and cap filament barbed ends with preferential affinity for ADP-bound ends. These processes add to a list of previously known properties of twinfilins, such as their interaction with capping proteins and the sequestration of G-actin, the latter established for G-actin without specification of the associated nucleotide (Paavilainen et al., 2004; Falck et al., 2004). In addition, Moseley et al. (2006) have shown that twinfilin also functions as a fragmenting protein by demonstrating that in an acidic environment ($pH < 6$) budding yeast twinfilin fragments actin filaments and promotes rapid turnover of actin.

Helfer et al. (2006) investigated the capping and sequestering activity of mammalian twinfilin in F-actin growth assays with a view toward understanding the effect of twinfilin on both the filament growth dynamics *and* the steady-state assembly of filaments. The capping of barbed ends by twinfilin was established in a number of experiments. Like other barbed-end capping proteins, twinfilin inhibits dilution-induced depolymerization of filamentous actin at the barbed ends. Moreover, twinfilin inhibits barbed-end growth in a range of concentrations substoichiometric to G-actin, which suggests that capping is the dominant mechanism responsible for the inhibition of

☆Research supported by NSF Grant 0517884.
*Corresponding author. Present address: Department of Mathematics, The Ohio State University, Columbus, OH 43210, USA.
Tel.: +1 614 292 9556.
E-mail address: tasos@math.ohio-state.edu (A. Matzavinos).

0022-5193/$ - see front matter © 2007 Elsevier Ltd. All rights reserved.
doi:10.1016/j.jtbi.2007.08.018

barbed-end growth. In contrast, the growth assay experiments reported by Helfer et al. (2006) show that the inhibition of pointed-end growth by twinfilin is due solely to the actin sequestering activity of the latter. Hence, although twinfilin inhibits growth totally at either end in a saturation manner, it caps only at the barbed end.

In order to demonstrate that twinfilin sequesters predominantly ADP-G-actin, Helfer et al. (2006) investigated the growth of filaments under three different experimental conditions: (a) in the absence of any accessory protein but gelsolin, (b) under the addition of thymosin $\beta 4$, which sequesters ATP-G-actin, and (c) in the presence of twinfilin. Filament growth in all cases is seeded by gelsolin-actin. Under these conditions barbed ends of actin filaments are capped by gelsolin, prohibiting capping by twinfilin to interfere with the dynamics. In cases (a) and (b) growth proceeds monotonically to a steady-state plateau. In contrast, in the presence of twinfilin the initial growth is followed by extensive depolymerization, as reflected by the initial increase in mean filament length followed by its decrease.[1] The authors assert that the latter type of biphasic evolution for filament length is not consistent with sequestration of ATP-G-actin alone and, hence, ADP-G-actin sequestration must be involved. The explanation they offer is that as the pointed ends of the filaments release ADP-actin monomers to the solution the latter are sequestered by twinfilin, which reduces the monomer pool that is available to the pointed ends. They show that this phenomenon is not manifested if twinfilin is replaced by thymosin $\beta 4$ since the latter sequesters ATP-G-actin and hence it rapidly equilibrates with the initially ATP-rich monomer pool.

Although this description is consistent with the observations, a quantitative model is needed to test the consequences of the underlying hypotheses on the integrated dynamics of the system. Specific issues that we address here concern the potential effect of gelsolin that has dissociated from filaments,[2] and the relative importance of gelsolin on the depolymerization dynamics as compared to the dynamics of twinfilin.

1.2. Computational approaches to stochastic chemical kinetics

Because actin-binding proteins typically interact differently with ATP- and ADP-actin, a complete description of the network involving reactions between actin monomers, filaments and actin-binding proteins must take into account the nature of the nucleotide at each monomer in an actin filament. In the following section we develop a stochastic simulation framework that incorporates this level of detail, yet allows us to efficiently simulate the temporal evolution of the filament length distribution under experimentally realistic conditions. Within this general framework we can study the effects of capping, sequestration and fragmentation proteins, using these proteins individually and in various combinations. This approach enables us to explain the dynamic behavior of the filament length distribution observed by Helfer et al. (2006) in the presence of twinfilin, and complements an earlier work (Hu et al., 2007) on the evolution of the length distribution *in vitro*. The algorithm we develop can also be applied to more efficiently simulate a large class of biologically important polymerization reactions.

Because the dynamics of individual filaments are important in a number of contexts, we treat the evolution of the composition of the mixture as a Markovian stochastic process, rather than as a deterministic process, and use the standard master equation formalism (cf. Gardiner, 1985; Gadgil et al., 2005). Thus, the system is characterized by the probability of being in a given state, and one is usually most interested in the first few moments of this distribution. The low-order moments can be found in essentially complete detail analytically for networks of linear reactions (Gadgil et al., 2005), but for other than first-order reactions the master equation is difficult to solve, either analytically or numerically. As a result Monte Carlo methods are used to generate realizations of the underlying stochastic process. For chemical reaction networks this is frequently done using one of the two stochastic simulation algorithms (SSAs), called the direct method and first reaction method, respectively, developed by Gillespie (1976). Various modifications of these two algorithms, aimed at improving the computational performance, have been developed (Gibson and Bruck, 2000; Cao et al., 2004; E et al., 2005) and the relative merits of various modifications have been evaluated by Cao et al. (2004).

All of these algorithmic approaches are formulated for the simulation of general reaction networks, without consideration of the underlying network topology. As we will see, a straightforward application of the direct method to the actin polymerization reaction network is not optimal, since the special structure associated with the polymerization reaction network is not used. The algorithm we develop makes optimal use of the network structure to minimize the computational cost of generating numerical realizations of the actin dynamics. Others have also developed stochastic mathematical models for the evolution of nucleotide compositions, but only under restrictions—such as conditions imposed on the filament length distribution and the actin monomer pool (cf. e.g. Bindschadler et al., 2004; Stukalin and Kolomeisky, 2006; Fass et al., 2007)—that are not needed in our formulation.

[1] Helfer et al. (2006) report pyrenyl-actin fluorescence, not filament length, but under their conditions there is no filament fragmentation and thus the two measures are equivalent.

[2] Helfer et al. (2006) assume that gelsolin remains bound to F-actin barbed ends throughout their experiment—a reasonable assumption if one considers the kinetic constants of capping by gelsolin and the absence of PIP_2 signaling that would facilitate the uncapping of filaments. Nonetheless, one of the aims of this paper is to confirm that the observed dynamics are intrinsic to the biochemical activity of twinfilin and not an outcome of gelsolin interference via capping.

2. Theory and algorithmic method

2.1. The master equation governing actin filament dynamics

Consider a solution of purified actin monomers and filaments under ionic conditions that support actin polymerization. In order to develop a master equation that embodies the state transitions in the system, we require a representation of the configuration or state of the system at each time. To uniquely define the state one must know the number of filaments of a given length, and, for each length present, the number of distinct nucleotide sequences in filaments and the number of filaments having one of these sequences. Thus, the state is characterized by a hierarchy of equivalence classes, first identifying filaments by their length, and, within an equivalence class of lengths, the number of filaments having a given nucleotide profile. These equivalence classes can be thought of as subpopulations of filaments, where a filament population is defined by the filament length *and* its nucleotide composition. For instance, the sequence

ATP – ADP – ADP – ADP

identifies a different filament population than

ATP – ATP – ADP – ADP

does. In this framework each filament population can be labeled by a finite string or sequence over a set that encodes the three distinct nucleotides. Here, we use the set $\mathscr{A} = \{1, 2, 3\}$, where one encodes ADP, two corresponds to the 'intermediate' nucleotide consisting of an ADP with a weakly associated phosphate, which is referred to as an ADP-Pi, and three encodes ATP.

The reactions that generate the state transitions can be regarded as the directed edges of a graph in which each vertex corresponds to an equivalence class or subpopulation of filaments. The vertices of this graph are labeled by finite sequences over $\mathscr{A}$, as shown by the example in Fig. 1. There a filament in the population corresponding to the sequence '33221' undergoes various transformations defined by the hydrolysis and phosphate release reactions (shown on the right part of the diagram), polymerization reactions (top and bottom parts of the diagram) and depolymerization reactions (left part of the diagram). For the polymerization reactions the nucleotide profile is irrelevant, and thus the finer equivalence class that identifies the profile is not needed.[3] As we see later, this makes our computational algorithm significantly more efficient.

Next we formulate the master equation for all admissible transitions in what may appear to be an overly abstract form, since the network structure itself is simple. However, this formulation serves as a blueprint for the data structures that are used in implementing an efficient simulation algorithm. Let $seq(\mathscr{A})$ be the set of all finite sequences over $\mathscr{A}$:

$$seq(\mathscr{A}) = \bigcup_{n\in\mathbb{N}} \mathscr{A}^n. \tag{1}$$

To characterize the state of the system at time t we have to specify the number of filaments in each population at this time. This is done by defining a function

$$\eta : seq(\mathscr{A}) \longrightarrow \mathbb{N}$$

which maps each finite sequence $\mathbf{s} = s_1 s_2 \ldots s_n \in seq(\mathscr{A})$—and consequently each population characterized by this sequence—to the total number of filaments characterized by $\mathbf{s}$. The configuration $\mathscr{C}$ of the system at time t is the number and type of all distinct filaments present in the system, and, since η encodes the configuration or state, it is called a *state variable*.

In a stochastic description of the system one can only determine the probability $P(\eta, t)$ of a state η, rather than the state itself. Accordingly, the master equation that describes the evolution of $P(\eta, t)$ encodes all transitions that alter P, and this can be written as

$$\frac{\partial}{\partial t} P(\eta, t) = \sum_{\zeta\in\mathscr{S}(\eta)} \mathscr{R}(\zeta, \eta) \cdot P(\zeta, t) \; - \sum_{\zeta\in\mathscr{T}(\eta)} \mathscr{R}(\eta, \zeta) \cdot P(\eta, t), \tag{2}$$

where η and ζ are state variables, $\mathscr{R}(\zeta, \eta)$ is the probability per unit time of a transition from state ζ to state η, and $\mathscr{R}(\eta, \zeta)$ is the probability per unit time of a transition from state η to state ζ. Here, $\mathscr{S}(\eta)$ is the set of all states that can terminate at η after one reaction step, and $\mathscr{T}(\eta)$ is the set of all states reachable from η in one step via feasible reactions; the notation is meant to suggest the 'source' and 'target' states at state η (Gadgil et al., 2005). Since there are only a finite number of chemical reactions, both $\mathscr{S}(\eta)$ and $\mathscr{T}(\eta)$

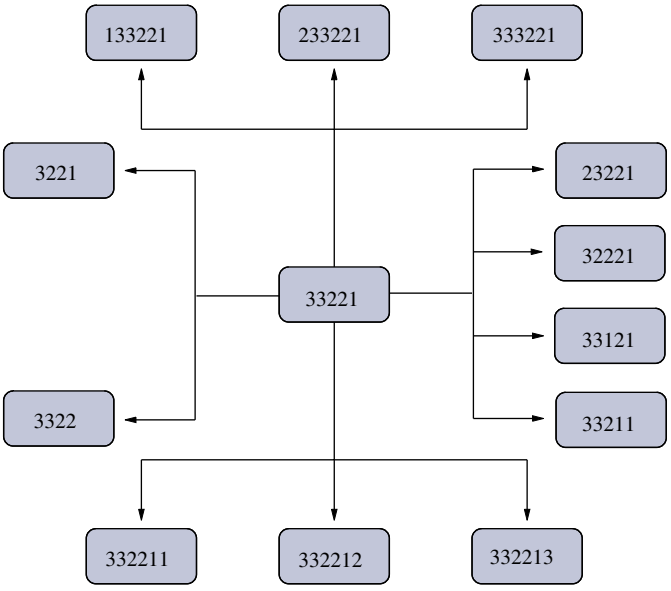

Fig. 1. State transition graph.

[3]The independence of the polymerization kinetic constants from the filament tip nucleotide state is assumed here, in accordance with Kuhn and Pollard (2005). Alternative possibilities are discussed in Fujiwara et al. (2007).

are finite and, hence, the sums appearing in Eq. (2) are finite.

To complete the description we have to specify the rate of increase $\mathscr{R}(\zeta,\eta)$ for $\zeta \in \mathscr{S}(\eta)$, and the rate of decrease $\mathscr{R}(\eta,\zeta)$ for $\zeta \in \mathscr{T}(\eta)$. We do this only for a polymerization and depolymerization at the barbed end; the reader can formulate the rates for other steps. To this end we introduce some notation. For every finite sequence

$$\mathbf{s} = s_1 s_2 \dots s_i \dots s_j \dots s_n \in seq(\mathscr{A}),$$

let $l(\mathbf{s})$ be the length n of $\mathbf{s}$, and let π_i^j be a 'projection' operator that selects the string $s_i \dots s_j$ from $\mathbf{s}$; thus

$$\pi_i^j(\mathbf{s}) = s_i \dots s_j. \tag{3}$$

When $i = j$—i.e. when the string represents a monomer—we denote the operator as π_i, i.e. $\pi_i^i \equiv \pi_i$. To orient the filaments we adopt the convention that s_1 defines the barbed end of $\mathbf{s}$ and s_n corresponds to the pointed end. Finally, the Dirac delta function over $seq(\mathscr{A}) \times seq(\mathscr{A})$ will be denoted by δ; its action is defined by

$$\delta(\mathbf{s}_1,\mathbf{s}_2) = \begin{cases} 1 & \text{if } \mathbf{s}_1 \equiv \mathbf{s}_2, \\ 0 & \text{otherwise,} \end{cases} \tag{4}$$

where identity of strings means equality component-wise.

Given a state η, we first have to determine the rates $\mathscr{R}(\zeta,\eta)$ corresponding to polymerization at the barbed end for every $\zeta \in \mathscr{S}(\eta)$. For this we first have to compute all $\zeta \in \mathscr{S}(\eta)$ from η. To do this we loop through all filament types in $\mathscr{C}$, and for each filament type in $\mathscr{C}$ encoded by a sequence $\mathbf{s}_0$ we generate a state $\zeta \in seq(\mathscr{A})$ by

1. increasing by one the size of the filament population that gave rise to $\mathbf{s}_0$ through a polymerization reaction at the barbed end,
2. increasing by one the monomer pool that contributed to the polymerization reaction and
3. subtracting one filament of type $\mathbf{s}_0$ from the current state η.

The result of these steps can be summarized by an operator $T_1^{\mathbf{s}_0}$ defined as follows. For each finite sequence $\mathbf{s}_0 \in seq(\mathscr{A})$, let $T_1^{\mathbf{s}_0}$ act on the state variable η as follows:

$$T_1^{\mathbf{s}_0}\eta(\mathbf{s}) = \eta(\mathbf{s}) - \overbrace{\delta(\mathbf{s},\mathbf{s}_0)}^{product} + \overbrace{\delta(\mathbf{s},\pi_2^{l(\mathbf{s})}(\mathbf{s}_0))}^{reactant} + \overbrace{\delta(\mathbf{s},\pi_1(\mathbf{s}_0))}^{monomer}. \tag{5}$$

The action of $T_1^{\mathbf{s}_0}$ on η yields a unique 'previous' state ζ, which generates η through the application of the barbed-end polymerization reaction on $\pi_2^{l(\mathbf{s})}(\mathbf{s}_0)$. Hence,

$$\mathscr{S}(\eta) = \{T_1^{\mathbf{s}_0}\eta \,|\, \mathbf{s}_0 \in supp(\eta)\}, \tag{6}$$

where $supp(\eta)$ is the set of non-empty equivalence classes of filaments characterized by their length and nucleotide profile. Formally,

$$supp(\eta) = \{\mathbf{s} \in seq(\mathscr{A}) \,|\, \eta(\mathbf{s}) > 0\}.$$

For $\mathbf{s} \in supp(\eta)$ and $\zeta \in \mathscr{S}(\eta)$ the probability per unit time of a $\zeta \to \eta$ transition, $\mathscr{R}(\zeta,\eta)$, is the product of the probability per unit time $c_{\pi_1(\mathbf{s})}$ of the specific polymerization step that defines the transition, and a combinatorial coefficient $h_{\mathbf{s}}$. The latter represents the number of independent combinations of monomers and filaments that can yield a filament of type $\mathbf{s}$ through a polymerization step. Thus,

$$\mathscr{R}(\zeta,\eta) = h_{\mathbf{s}} \cdot c_{\pi_1(\mathbf{s})}. \tag{7}$$

The state variables ζ and η uniquely define the finite sequence $\mathbf{s} \in seq(\mathscr{A})$. The probability per unit time $c_{\pi_1(\mathbf{s})}$ of a polymerization event depends on the type of monomer being added, i.e. on the nucleotide $\pi_1(\mathbf{s})$ bound to the monomer. The combinatorial coefficient $h_{\mathbf{s}}$ and the probability per unit time $c_{\pi_1(\mathbf{s})}$ are determined by the state variable $\zeta = T_1^{\mathbf{s}}\eta \in \mathscr{S}(\eta)$ and the deterministic rate constant of the polymerization step as

$$h_{\mathbf{s}} = T_1^{\mathbf{s}}\eta(\pi_1\mathbf{s}) \cdot T_1^{\mathbf{s}}\eta(\pi_2^{l(\mathbf{s})}\mathbf{s}) \quad \text{and} \quad c_{\pi_1(\mathbf{s})} = \frac{k_{\pi_1(\mathbf{s})}}{\mathscr{N}_A V}, \tag{8}$$

where $\mathscr{N}_A$ is Avogadro's number, V is the volume of the system and $k_{\pi_1(\mathbf{s})}$ is the rate constant for addition of a monomer having a $\pi_1(\mathbf{s})$ nucleotide.

Similar reasoning leads to the term due to polymerization steps leaving η, and it follows that the evolution of P due only to barbed-end polymerization is governed by

$$\frac{\partial}{\partial t}P(\eta,t) = \sum_{\mathbf{s}\in supp(\eta)} h_{\mathbf{s}} \cdot c_{\pi_1(\mathbf{s})} \cdot P(T_1^{\mathbf{s}}\eta, t) - \sum_{\mathbf{s}\in supp(\eta)} \left(\sum_{m\in\mathscr{A}} c_m \eta(m)\right) \eta(\mathbf{s}) P(\eta,t). \tag{9}$$

The simple form of these terms stems from the fact that the addition of a monomer depends only on the monomer type, not on what is on the filament end (cf. Table 1). The contribution of depolymerization at η to the master equation is derived shortly, and the remaining reactions such as ATP hydrolysis, phosphate release and filament fragmentation can be treated similarly.

2.2. An efficient SSA for polymerization reactions

The main difficulty associated with using the direct method for simulating the actin polymerization network is the potentially large number of new species that are created due to growth and decay of filaments, and to changes in the nucleotide compositions of filaments due to hydrolysis. Since each site in a filament can contain one of the three nucleotides, there are potentially 3^n distinct species for a filament of length n. In the direct method one decides which reaction will occur next and when based on all possible reaction rates in the system. Thus, the emergence of a large number of new filament types in the system will increase the computational cost due to the complexity associated with processing a large set of non-zero reaction rates. However, a careful examination of the master equation as we have formulated it reveals the possibility of an efficient grouping of the rates in a way that can

Table 1
Rate constants and literature sources

Description of kinetic constant	Symbol	Value	References
ADP-G-actin polymerization at barbed ends	k_{bD}^{+}	$3.8\,\mu M^{-1}\,s^{-1}$	Kuhn and Pollard (2005)
ATP-G-actin polymerization at barbed ends	k_{bT}^{+}	$7.4\,\mu M^{-1}\,s^{-1}$	Kuhn and Pollard (2005)
ADP-actin depolymerization from barbed ends	k_{bD}^{-}	$1.5\,s^{-1}$	Kuhn and Pollard (2005)
ADP-Pi-actin depolymerization from barbed ends	$k_{bD\cdot Pi}^{-}$	$0.9\,s^{-1}$	Kuhn and Pollard (2005)
ATP-actin depolymerization from barbed ends	k_{bT}^{-}	$0.9\,s^{-1}$	Kuhn and Pollard (2005)
ADP-G-actin polymerization at pointed ends	k_{pD}^{+}	$0.16\,\mu M^{-1}s^{-1}$	Kuhn and Pollard (2005)
ATP-G-actin polymerization at pointed ends	k_{pT}^{+}	$0.56\,\mu M^{-1}s^{-1}$	Kuhn and Pollard (2005)
ADP-actin depolymerization from pointed ends	k_{pD}^{-}	$0.26\,s^{-1}$	Kuhn and Pollard (2005)
ADP-Pi-actin depolymerization from pointed ends	$k_{pD\cdot Pi}^{-}$	$0.19\,s^{-1}$	Kuhn and Pollard (2005)
ATP-actin depolymerization from pointed ends	k_{pT}^{-}	$0.19\,s^{-1}$	Kuhn and Pollard (2005)
ATP hydrolysis on polymerized actin		$0.3\,s^{-1}$	Blanchoin and Pollard (2002)
Phosphate release from filamentous ADP-Pi-actin		$0.0026\,s^{-1}$	Bindschadler et al. (2004)
ADP exchange for ATP on globular actin	$k_{D\to T}$	$0.01\,s^{-1}$	Selden et al. (1999)
Depolymerization of trimers		$10^{3}\,s^{-1}$	Sept et al. (1999)
Depolymerization of dimers		$10^{6}\,s^{-1}$	Sept et al. (1999)
Binding of ADP-G-actin by twinfilin	k_{sqD}^{+}	$180\ \mu M^{-1}s^{-1}$	Helfer et al. (2006)
Release of ADP-G-actin from twinfilin	k_{sqD}^{-}	$1.8\,s^{-1}$	Helfer et al. (2006)
Capping of ADP-actin barbed ends by twinfilin	k_{cpD}^{+}	$10.0\,\mu M^{-1}s^{-1}$	Assigned estimate (see text)
Release of twinfilin from ADP-actin barbed ends	k_{cpD}^{-}	$1.0\,s^{-1}$	Assigned estimate
Capping of ADP-Pi-actin barbed ends by twinfilin	$k_{cpD\cdot Pi}^{+}$	$1.0\,\mu M^{-1}s^{-1}$	Assigned estimate
Release of twinfilin from ADP-Pi-actin barbed ends	$k_{cpD\cdot Pi}^{-}$	$10.0\,s^{-1}$	Assigned estimate
Capping of ATP-actin barbed ends by twinfilin	k_{cpT}^{+}	$1.0\,\mu M^{-1}s^{-1}$	Assigned estimate
Release of twinfilin from ATP-actin barbed ends	k_{cpT}^{-}	$10.0\,s^{-1}$	Assigned estimate

drastically reduce the computational complexity of the algorithm. To see this, suppose that the state of the system at time t is η, and, in order to demonstrate the basic idea, consider only depolymerization reactions at the barbed end of a filament. The target states $\mathscr{T}(\eta)$ reachable from η can be defined by an appropriate operator as was done for the source states in the case of the polymerization reaction, and the decrease of P due to these steps evolves according to

$$\frac{\partial}{\partial t}P(\eta,t) = -\sum_{\zeta\in\mathscr{T}(\eta)}\mathscr{R}(\eta,\zeta)\cdot P(\eta,t) = -\sum_{\mathbf{s}\in supp(\eta)}h_{\mathbf{s}}c_{\mathbf{s}}\cdot P(\eta,t). \tag{10}$$

Since depolymerization is a first-order reaction, the combinatorial coefficient $h_{\mathbf{s}}$ is simply equal to the number of filaments of type $\mathbf{s}$ in the configuration $\mathscr{C}$. In particular,

$$h_{\mathbf{s}} = \eta(\mathbf{s}) \quad \text{and} \quad c_{\mathbf{s}} = k^{-}_{\pi_1(\mathbf{s})}, \tag{11}$$

where $k^{-}_{\pi_1(\mathbf{s})}$ is the deterministic rate constant for the release of a $\pi_1(\mathbf{s})$ monomeric unit from the barbed end of a filament. It is known that $k^{-}_{\pi_1(\mathbf{s})}$ depends only on the outermost nucleotide $\pi_1(\mathbf{s})$ and not on the 'inner' composition of the filament (Kuhn and Pollard, 2005), hence, $c_{\mathbf{s}} = c_{\pi_1(\mathbf{s})}$. It follows that by re-organizing the sum in Eq. (10), this equation can be written as

$$\frac{\partial}{\partial t}P(\eta,t) = -\sum_{m\in\mathscr{A}}h_m c_m\cdot P(\eta,t), \tag{12}$$

where h_m is the number of filaments in $\mathscr{C}$, of which the outermost nucleotide at the barbed end is of type $m\in\mathscr{A}$.

Eq. (12) shows that the distinction of the depolymerization reaction rates associated with all different species characterized by sequences $\mathbf{s}\in seq(\mathscr{A})$ is not necessary for this particular step; one can characterize the depolymerization dynamics by investigating the evolution of three first-order pseudoreactions acting on the pseudospecies

$$\mathscr{P}_m = \{\mathbf{s}\in supp(\eta)|\pi_1(\mathbf{s}) = m\}, \tag{13}$$

where $m\in\mathscr{A}$. The collection of the sets $\mathscr{P}_m$ provides a coarsening of the equivalence classes defining the state of the configuration $\mathscr{C}$. In effect, Eq. (12) defines a depolymerization pseudoreaction acting on the pseudospecies $\mathscr{P}_m$, with the rate of the reaction given by $h_m c_m$. This setting contains all the necessary information for applying Gillespie's direct method on the coarse decomposition of $\mathscr{C}$ given by the pseudospecies $\mathscr{P}_m$.

This 'lumping' of species significantly reduces the size of the data set of reaction rates that would have to be generated and manipulated in order to simulate the system using the standard direct method. It is based on the particular structure of the kinetic network and can be applied, by defining appropriate pseudoreactions, to virtually all reactions in the system. For instance, all hydrolysis reactions can be represented by a generic hydrolysis pseudoreaction, the rate of which is determined by the rates of the individual component reactions.

By using this observation, we have developed and implemented an efficient variant of Gillespie's SSA for the actin network, and we have compared the performance of this implementation with the performance of an implementation based on Gillespie's direct method. Both implementations were written in the C programming language and the timing was performed on a dual-core processor computer system running at approximately 2.4 GHz.

An experimental configuration of a volume of 1000 μm^3 was assumed and the admissible reactions were polymerization and depolymerization, nucleotide hydrolysis, release of phosphate and exchange of ADP for ATP on G-actin. The nucleation reaction was assumed to be shut off. The experiments were performed for various initial concentrations of filament seeds. The initial concentration of ATP-G-actin was 2.5 μM, and the stopping criterion for the timing of the computational performance was a fixed elapsed time of 100 s for polymerization.

Fig. 2 shows the results of the timing of the two implementations. As can be seen, for an initial number of 10^3 actin filaments, the optimized SSA reaches 100 s of experimental time within ~17 s of CPU time, whereas Gillespie's SSA requires ~3600 s of CPU time. It is well known that the computational cost of Gillespie's direct method depends linearly on the number of reactions present in the system (Cao et al., 2004). However, this result applies to reaction networks with a constant number of reactions, whereas in the system under discussion the number of filament species in the configuration $\mathscr{C}$—and consequently the number of corresponding reactions—increases with time. This explains the apparently exponential computational cost of the direct method in this setting. In contrast, our optimized approach manifests a linear dependence, since the number of the defined pseudospecies remains constant throughout the execution of the algorithm.

3. Results

3.1. Understanding the ADP-G-actin sequestering activity of twinfilin

In order to demonstrate experimentally that twinfilin sequesters predominantly ADP-G-actin, Helfer et al. (2006) studied the growth of filaments under three different experimental conditions: (a) in the absence of any accessory protein but gelsolin, (b) under the addition of thymosin $\beta 4$, which sequesters ATP-G-actin, and (c) in the presence of twinfilin. In all the three cases, filament growth is seeded by gelsolin-actin and is assayed by the intensity of pyrenyl-actin fluorescence. The authors assume that barbed ends of actin filaments are capped by gelsolin, which precludes barbed-end capping by twinfilin to interfere with the dynamics. In cases (a) and (b) growth proceeds monotonically to a steady-state plateau, whereas, in the presence of twinfilin, the initial growth is followed by extensive depolymerization. The authors conclude that the latter type of biphasic evolution of filament length is not consistent with sequestration of ATP-G-actin alone and, therefore, that ADP-G-actin sequestration must be present. The explanation they offer is that as the pointed ends of the filaments give up ADP-actin monomers to the solution the latter are sequestered by twinfilin, which

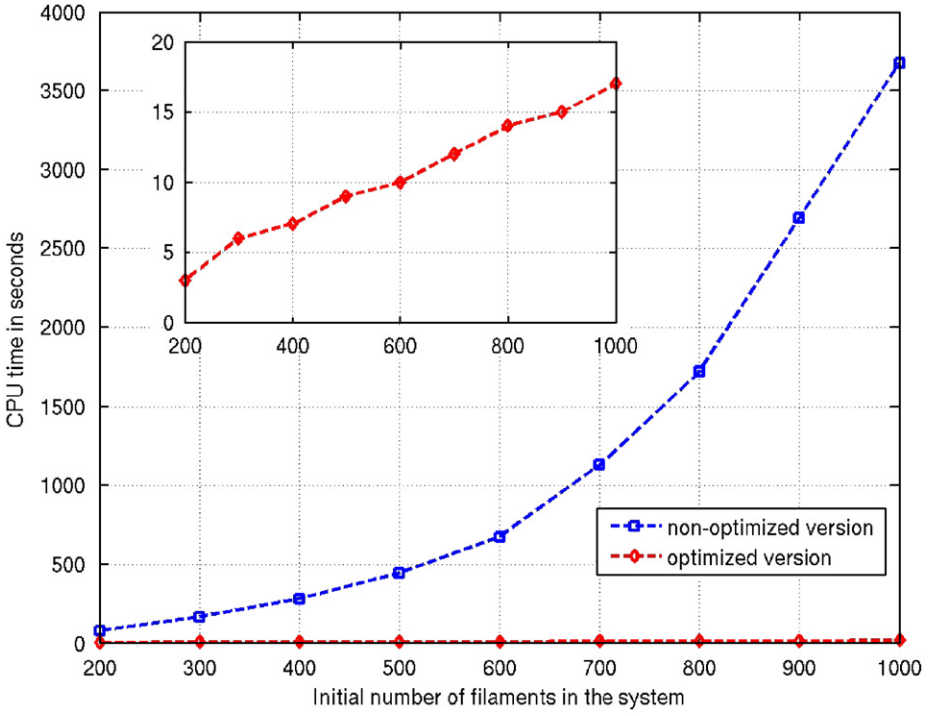

Fig. 2. Timing of Gillespie's stochastic simulation algorithm versus our optimized method.

reduces the monomer pool that is available to the pointed ends. This phenomenon is not manifested if twinfilin is replaced by thymosin $\beta 4$ since the latter sequesters ATP-G-actin and it rapidly equilibrates with the initially ATP-rich monomer pool.

Although this description is plausible, a quantitative model that can reproduce the observed time course of polymerization and which can be used to assess the importance of various assumptions is not provided by Helfer et al. (2006). In particular, the conclusions reached are predicated on the assumption that the biphasic growth behavior is not an outcome of gelsolin interference through a possible fragmenting activity or by interference with the pointed-end dynamics. In this section we assess the relative importance of gelsolin on the emergence of biphasic dynamics. We demonstrate computationally that the addition of a generic ADP-G-actin sequestering protein into a solution of actin filaments suffices, under certain conditions, to induce biphasic growth behavior. Hence, we conclude that, although gelsolin interference may quantitatively perturb the dynamics, its presence in the medium is not necessary for the establishment of the dynamic behavior reported by Helfer et al. (2006).

The rationale behind using gelsolin-actin seeded growth is to distinguish between the monomer sequestration activity of twinfilin and its capping activity, by essentially blocking the twinfilin binding site on F-actin. In interpreting data from polymerization assays of gelsolin-actin seeds, Helfer et al. (2006) assume that filament barbed ends remain capped throughout the time course of the experiments. This assumption is based on the high affinity of gelsolin for barbed ends, although a chemical equilibrium presumably does develop and, hence, there should be uncapped filaments that contribute to the evolution of the dynamics. To investigate the dynamics of the system under the assumptions made by the authors, we performed a numerical experiment focusing on pointed-end polymerization dynamics under the effect of a generic G-ADP-actin sequestering protein. The experiment consists of introducing various concentrations of the sequestering protein up to a concentration of $5.4\,\mu M$, the concentration of mammalian twinfilin used by Helfer et al. (2006).

Although mammalian twinfilin exhibits a weak tendency to sequester ATP-G-actin, it has a ~10-fold higher affinity for ADP-G-actin (Ojala et al., 2002; Helfer et al., 2006). It is also well documented in the literature that all twinfilins sequester predominantly ADP-G-actin at steady state in solutions containing ATP. Since we are interested in identifying minimal dynamic behaviors that can reproduce the experimental dynamics, we focus on the role of the ADP-G-actin sequestering activity of twinfilin. Hence, we neglect ATP-G-actin sequestration, and, by simulating a generic ADP-G-actin sequestering protein, we will demonstrate that the former is not necessary for the emergence of biphasic growth dynamics. Indeed, as we will see, the emergence of a biphasic evolution for the filament length distribution is an intrinsic property of the sequestering dynamics of twinfilin in the sense that neither the capping activity of the latter nor the possible fragmentation activity by the gelsolin present in the medium is necessary for the establishment of the specific dynamics. In the following we will not distinguish between the generic ADP-G-actin sequestering protein, the dynamics of which we investigate, and twinfilin unless it is necessary. The kinetic constants used for the ADP-G-actin binding to twinfilin and for other steps in the mechanism are given in Table 1. The kinetic constants for the capping activity of twinfilin were assigned in accordance with the equilibrium constants reported by Helfer et al. (2006). The polymerization rates are those of Kuhn and Pollard (2005), who investigate the polymerization of Mg-actin, whereas the growth assays of Helfer et al. (2006) have been done with Ca-actin. We know of no experimental data for polymerization of Ca-actin that establish rates for monomers with different associated nucleotides in the detail done for Mg-actin in Kuhn and Pollard (2005).

Figs. 3(a)–(d) show scatter plots of the evolution of the filament length distribution in the presence of various concentrations of twinfilin. Since the barbed ends of filaments in this experiment are assumed capped by gelsolin, only the pointed ends contribute to the polymerization dynamics, and the only activity of twinfilin is the sequestration of ADP-G-actin. The initial conditions for the simulations reflect the experimental values used by Helfer et al. (2006). Polymerization of $2.5\,\mu M$ of monomeric actin associated with ATP was seeded by $6\,nM$ of gelsolin-actin.

It is evident that the ADP-G-actin sequestration by twinfilin dramatically alters the advection–diffusion dynamics manifested in the absence of twinfilin, as shown in Fig. 3(a) and analyzed by Hu et al. (2007). In the presence of $5.4\,\mu M$ of twinfilin the actin filaments depolymerize completely within approximately 3×10^3 s. However, experimentally the same concentration of twinfilin produces results that are qualitatively similar to the evolution shown in Fig. 3(b). This might be due to the different kinetic constants used for the polymerization reaction network (Mg-actin versus Ca-actin). Alternatively, the weak sequestration of ATP-G-actin by twinfilin might be responsible for the discrepancy between the simulations and the experimental data. To test this we have simulations (not shown) where, in the presence of a weak ATP-G-actin sequestration activity, twinfilin equilibrates rapidly with the initially ATP-rich monomer pool. Hence, the concentration of free twinfilin available for ADP-actin sequestration on the time scale of the establishment of an ADP-G-actin pool is effectively reduced. This implies that the complete depolymerization of actin filaments, as shown in Fig. 3(d), can be effectively controlled by the kinetics of the ATP-G-actin sequestration activity.

Some insights into how the gradual introduction of twinfilin induces the observed biphasic evolution in time are gained from the dynamics of the ADP- and ATP-G-actin pools shown in Figs. 4(a)–(d). The steady-state levels

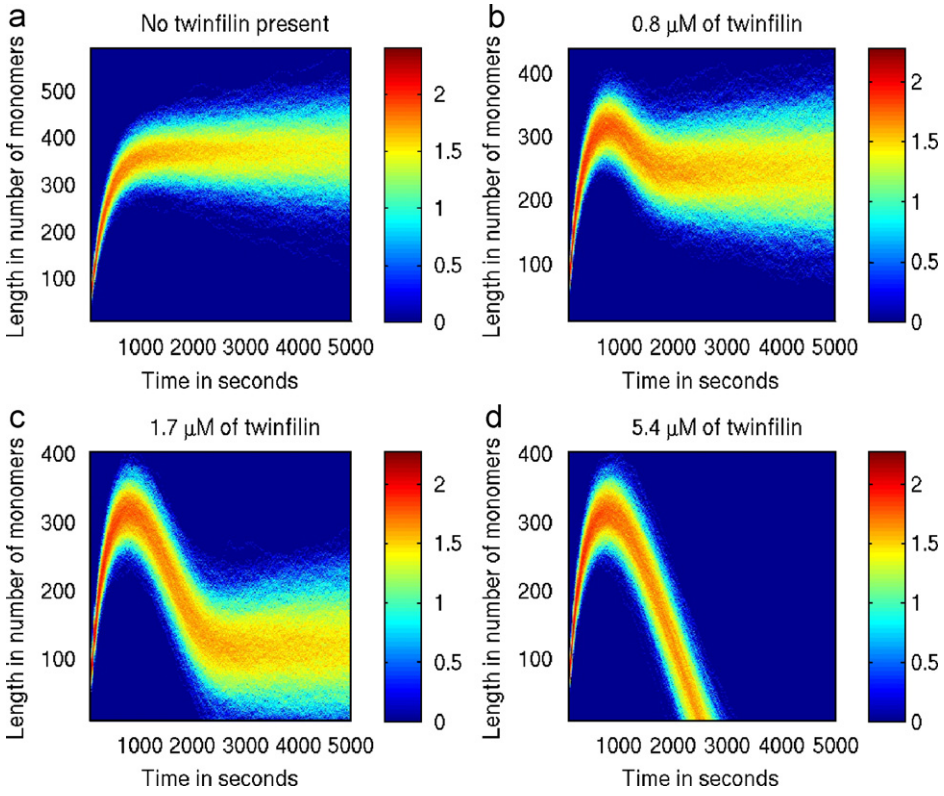

Fig. 3. Evolution in time of gelsolin-actin seeded filament growth (a) in the absence of twinfilin, (b) in the presence of 0.8 μM of twinfilin, (c) in the presence of 1.7 μM of twinfilin and (d) in the presence of 5.4 μM of twinfilin. The sole biochemical activity of twinfilin in this experiment is the sequestration of ADP-G-actin. The color code is on a logarithmic scale.

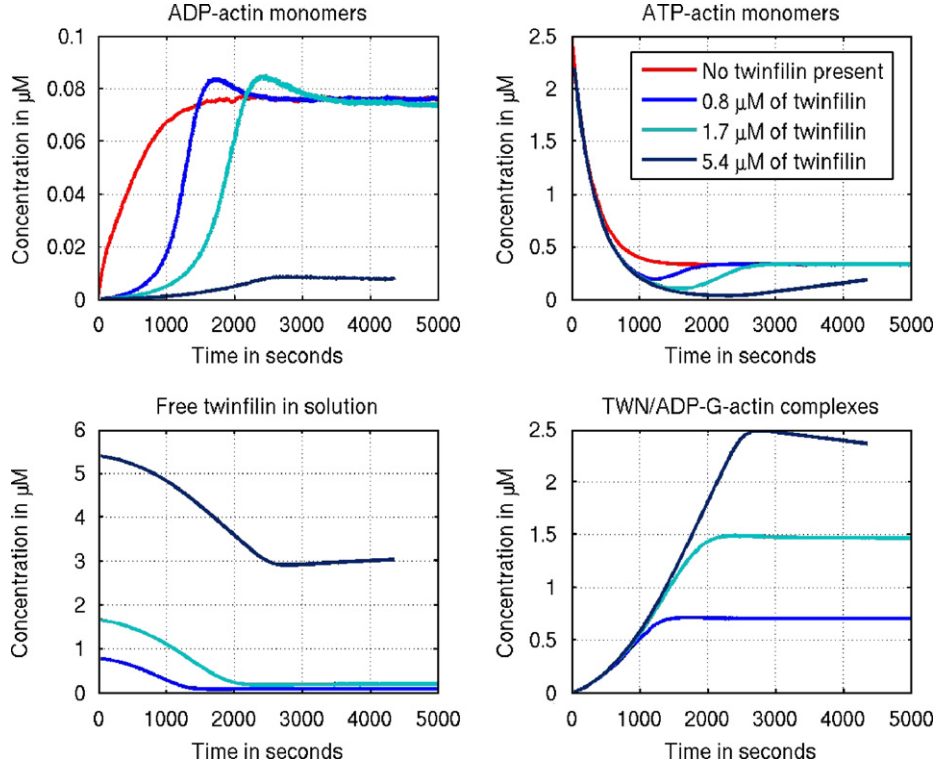

Fig. 4. Evolution in time of (a) the ADP-actin monomer pool, (b) the ATP-actin monomer pool, (c) free twinfilin in solution and (d) the TWF/ADP-G-actin pool.

of ADP- and ATP-G-actin are shown in Figs. 4(a) and 4(b), respectively. Interestingly enough, as twinfilin sequesters part of the emerging ADP-actin pool—a process depicted in Fig. 4(d)—the ATP-actin concentration levels undershoot the corresponding steady-state level. This can be understood with reference to Fig. 5, where the species are lumped into six pools: ADP-G-actin monomers, ATP-G-actin monomers, uncapped filaments, filaments capped by twinfilin, twinfilin/ADP-G-actin complexes and free twinfilin. Fig. 5 shows the fluxes between these pools in the more complex experimental setting, where filament barbed ends are available for capping by twinfilin. When all barbed ends are capped by gelsolin, the part of the diagram that corresponds to the capping activity of twinfilin is not relevant, since the corresponding fluxes are zero. However, it will be used in a subsequent analysis of capping.

The experimentally determined values of the kinetic constants in the schematic diagram indicate that, as the ADP-G-actin pool gradually emerges, it rapidly gets sequestered by twinfilin. Since the flux associated with the exchange of an ADP for an ATP on G-actin is negligible, as compared to the one that corresponds to ADP-G-actin sequestration, the system is driven below the steady-state level of ATP-G-actin. This triggers extensive depolymerization at the pointed end following the initial burst of polymerization. As Figs. 3(b)–(d) and 4(b) show, the onset of the phase of extensive depolymerization coincides temporally with the emergence of ATP-G-actin population levels below the steady-state value.

The extensive depolymerization of filaments results in an enhanced flux from the filament pool to the ADP-G-actin pool. This, in conjunction with the bottleneck in the D → T transition shown in Fig. 5, results in the accumulation of ADP-G-actin, leading to an overshoot above the ADP-G-actin steady-state level. As shown in Fig. 4(a) the latter phenomenon is transient and is initiated *after* the system has entered the depolymerization regime of the dynamics. Eventually, monomer sequestration and the slow D → T reaction drive the monomer subpopulations toward steady-state values and the system toward the diffusive dynamics analyzed by Hu et al. (2007).

These results explain the biphasic evolution of the filament length distribution. They also indicate that by controlling the concentration of twinfilin one may be able to modify the time scale on which ADP-actin levels are above the corresponding steady-state level. This could potentially induce an extensive polymerization phase following the depolymerization dynamics, with the former resulting in a distribution of larger filaments. Indeed, such dynamics are feasible, as is shown in Figs. 6(a) and (b). The simulation underlying these figures has been performed

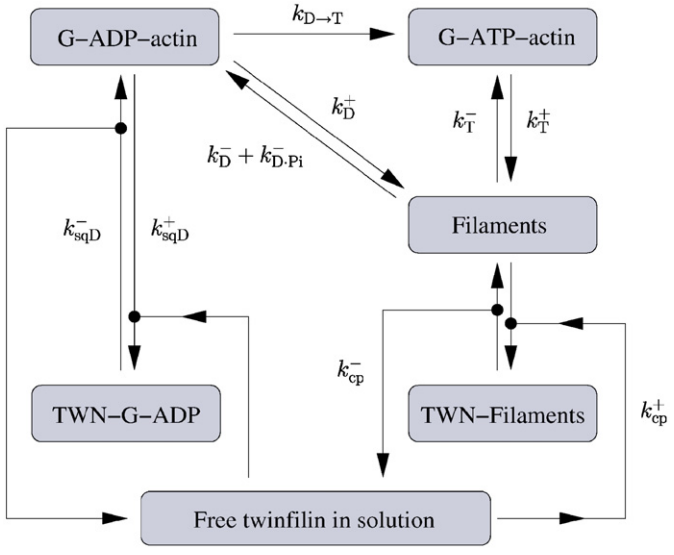

Fig. 5. A schematic diagram for the reaction network of actin monomers, filaments and twinfilin. The kinetic constants appearing in the diagram are defined as follows: $k_T^{\pm} = k_{bT}^{\pm} + k_{pT}^{\pm}$, $k_D^{\pm} = k_{bD}^{\pm} + k_{pD}^{\pm}$, $k_{D\cdot Pi}^{-} = k_{bD\cdot Pi}^{-} + k_{pD\cdot Pi}^{-}$ and $k_{cp}^{\pm} = k_{cpD}^{\pm} + k_{cpD\cdot Pi}^{\pm} + k_{cpT}^{\pm}$. A description of the notation and the numeric values of the kinetic constants can be found in Table 1.

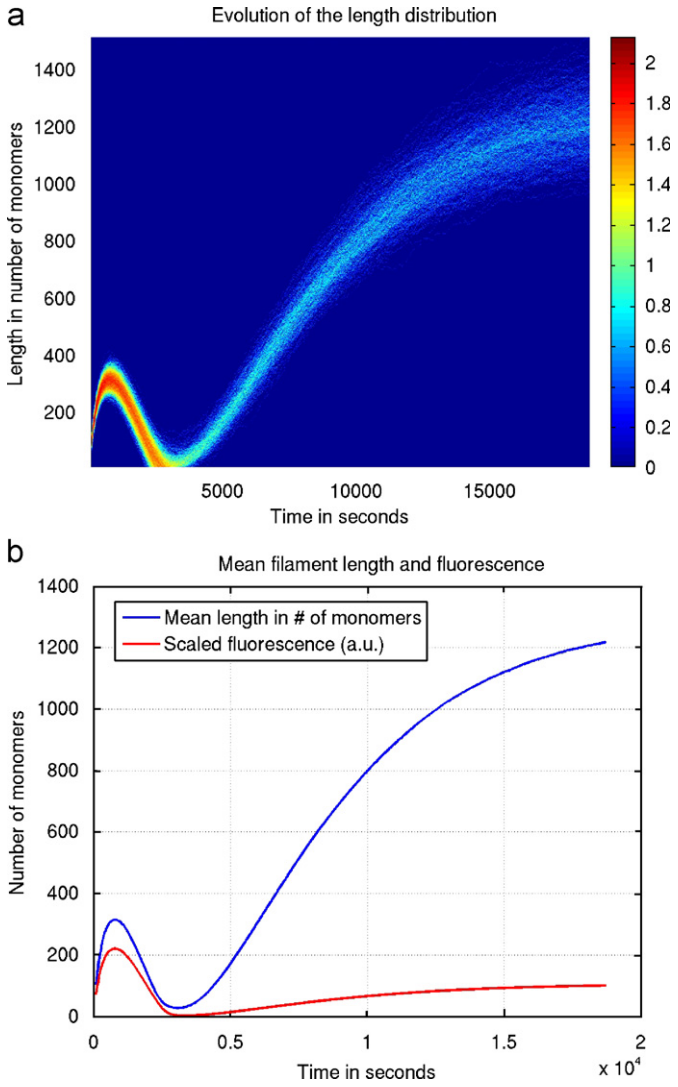

Fig. 6. (a) Evolution of the filament length distribution in the presence of 2.75 μM of twinfilin and (b) evolution in time of the mean filament length in blue and simulated pyrenyl-actin fluorescence (which is emitted only when monomers are in filaments) in arbitrary units in red.

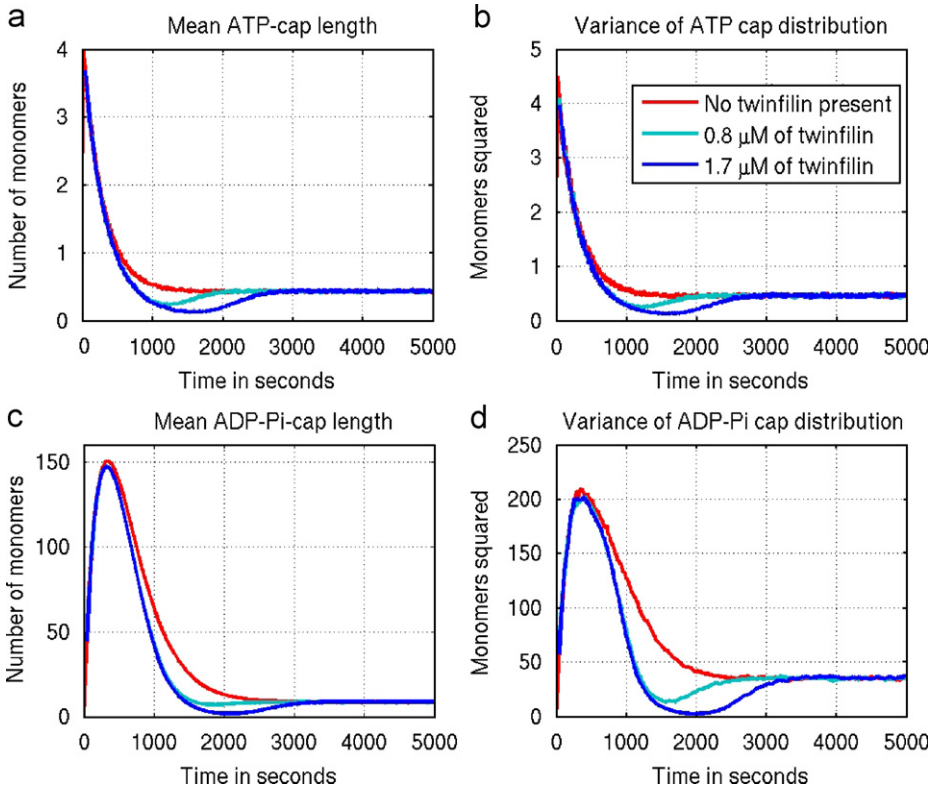

Fig. 7. Evolution in time of (a) the mean ATP cap length, (b) the variance of the ATP-cap length distribution, (c) the mean ADP-Pi cap length and (d) the variance of the ADP-Pi-cap length distribution.

under the same experimental conditions that correspond to 3(a)–(d), but: the concentration of twinfilin is 2.75 μM. As shown in Fig. 6(a), the latter concentration fails to induce complete depolymerization of the whole filament distribution, as in the case of Fig. 3(d). Nonetheless, a significant number of filaments do depolymerize completely and, as a result, the emerging enhanced population of ADP-actin monomers induces the extensive polymerization of the remaining filaments. Fig. 6(b) shows the evolution of the mean filament length and the corresponding simulated pyrenyl-labeled fluorescence experiment, and from this it is clear that fluorescence experiments of this type would fail to detect the emergence of a population of large filaments, since the fluorescence signal would weaken due to the loss of a significant number of filaments in the depolymerization regime of the dynamics. These dynamics suggest that the twinfilin family of proteins can be an essential part of a molecular machinery that implements a control mechanism regulating filament lengths after a short burst of polymerization.

Various characteristics of the system that are not accessible in the experimental setting of Helfer et al. (2006) can be investigated in the computational framework developed here. For instance, we have analyzed the nucleotide compositions of filaments throughout the various dynamic regimes of the numerical experiments underlying Figs. 3(a)–(d). Since the barbed ends are constantly capped by gelsolin, the only reactions affecting nucleotide compositions are the polymerization and depolymerization of monomers at the pointed ends, the hydrolysis of ATP on F-actin and the subsequent release of phosphates. We find that throughout the time course of the assay, the filaments develop large ADP-actin cores with ADP-Pi caps at the pointed ends, the length of which varies significantly in the polymerization, depolymerization and diffusion-dominated regimes of the dynamics, as expected. Occasionally, small ATP-actin monomer caps are formed as well, but they do not persist. The statistics of ADP-Pi- and ATP-actin cap sizes are shown in Figs. 7(a)–(d), and as can be seen there, the maximum size of ADP-Pi cap length is approximately 150 monomers on average with a deviation of ~14 monomers. In the diffusive regime of the dynamics the average size of ADP-Pi caps is approximately 10 monomers long with a deviation of 6 monomers.

3.2. *Unraveling the dynamic effects of the different biochemical activities of twinfilin*

The capping of barbed ends by twinfilin was established by Helfer et al. (2006), and, like other capping proteins, twinfilin inhibits dilution-induced depolymerization of filamentous actin at the barbed ends. Moreover, it inhibits barbed-end growth in a range of concentrations substoichiometric to G-actin, which cannot be attributed to sequestration of actin by twinfilin alone and suggests that capping is the dominant mechanism responsible for the inhibition of growth.

A question that arises from these findings is whether the biphasic dynamics discussed earlier persist under conditions in which barbed ends can be capped by twinfilin. This was inhibited in the Helfer et al. (2006) experiments by the capping of barbed ends with gelsolin. The question of whether the biphasic evolution only exists under the specific conditions used there, or whether it is an intrinsic property of the specific activities of twinfilin—and, if so, which of them—was addressed in the framework of our computational approach. As a first step we investigated the type of dynamics that emerge in the absence of gelsolin and under the influence of specific subsets of twinfilin actions.

Figs. 8(a)–(d) show the results of numerical computations simulating a modification of the experiments shown in Figs. 3(a)–(d). Initially, all filament seeds were uncapped, i.e. there was no gelsolin in the medium. This configuration allows for the capping activity of twinfilin in addition to ADP-G-actin sequestration. Twinfilin caps filament barbed ends with a preferential binding to those associated with ADP. The chemical affinities of a weak binding reaction between twinfilin and barbed ends associated with ATP or ADP-Pi have also been reported by Helfer et al. (2006), and have been incorporated in our numerical computations. Figs. 8(a)–(d) show scatter plots of the evolution of the filament length distribution under various conditions. It is evident that the biphasic growth of gelsolin-actin seeds in the presence of twinfilin, reported by Helfer et al. (2006) and analyzed in this article, is also present in the absence of gelsolin, albeit on a different time scale. The latter difference is due to the faster polymerization kinetics at the uncapped barbed ends. These results demonstrate that the biphasic evolution of the length distribution is intrinsic to the dynamics of the interactions of twinfilin with actin. Although gelsolin interference may quantitatively perturb the dynamics, its presence in the medium is not necessary to obtain the biphasic evolution. Our computational framework also enables us to observe various characteristics of the system which would not be directly observable in the experimental setting of growth assays. Fig. 9(a) shows the evolution in time of the percentage of filaments that are capped by twinfilin. As expected, increasing concentrations of twinfilin lead to increasing numbers of capped filaments. Interestingly enough, in the presence of 0.8 and 1.7 μM of twinfilin the equilibration of the population of capped filaments coincides in time with the initiation of the diffusion-dominated regime of the dynamics.

In these experiments barbed ends compete with ADP-G-actin for twinfilin, and the gradual establishment of an ADP-G-actin pool through enhanced depolymerization is responsible for the reduction of the population of capped filaments. These dynamics provide an example of a mechanism for dynamic uncapping of filaments. Indeed, the competition of filaments and monomers for the cap

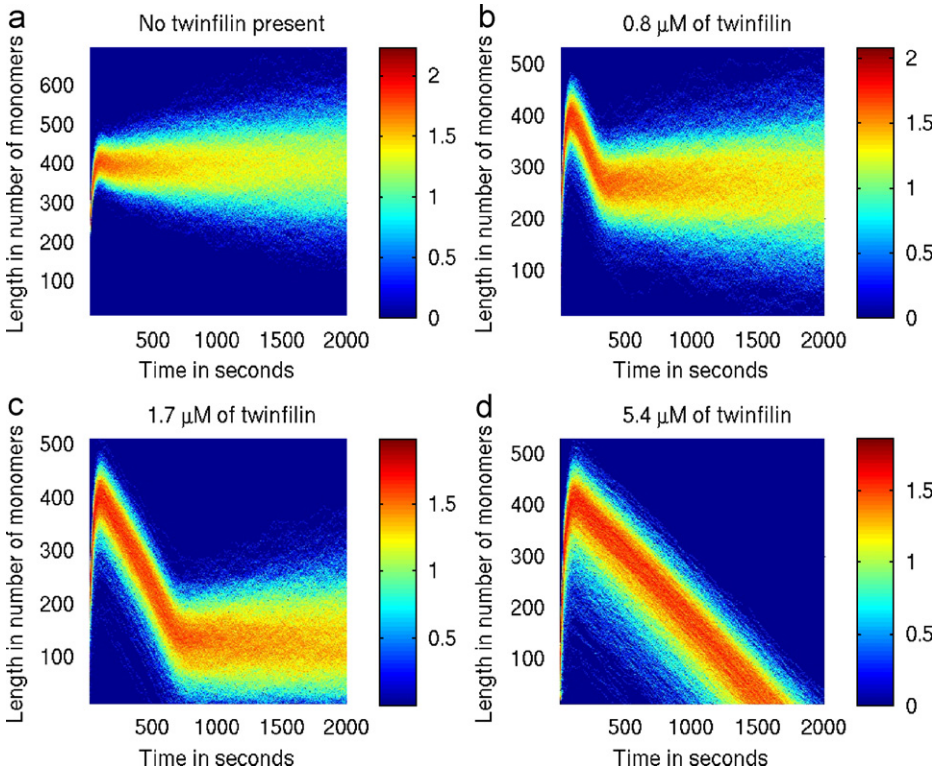

Fig. 8. Evolution in time of the filament length distribution (a) in the absence of twinfilin, (b) in the presence of 0.8 μM of twinfilin, (c) in the presence of 1.7 μM of twinfilin and (d) in the presence of 5.4 μM of twinfilin. Initially, all filament seeds are uncapped, i.e. there is no gelsolin in the medium. The biochemical activities of twinfilin in this experimental setting include sequestration of ADP-G-actin and filament barbed-end capping. The color code is on a logarithmic scale.

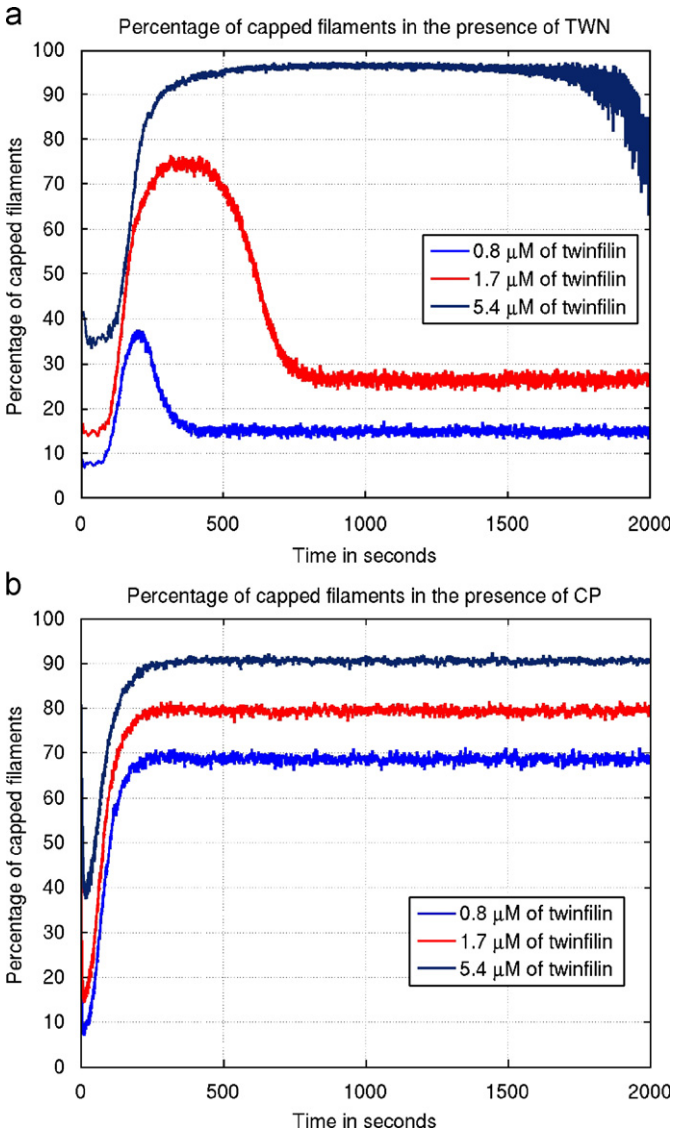

Fig. 9. Evolution in time of the percentage of filaments that are capped by (a) twinfilin that functions both to cap and sequester and (b) twinfilin that only caps filament.

leads to the control of the population of capped filaments through the concentration of ADP-G-actin monomeric units. Fig. 9(a) demonstrates this and is to be contrasted to Fig. 9(b) which shows the evolution of the capped filament population in the presence of a capping protein with the same capping kinetics as twinfilin, but with no monomer sequestering activity. These results can be understood in terms of the fluxes in the schematic diagram shown in Fig. 5. The flux from the ADP-G-actin pool to the twinfilin/ADP-G-actin pool is greatly enhanced by the elevation of the ADP-G-actin concentration, and, consequently, the balance between twinfilin/ADP-G-actin complexes and filaments capped by twinfilin shifts toward the former.

In order to identify the specific action of twinfilin that leads to the biphasic growth, we did a sequence of numerical experiments in which various attributes of twinfilin were isolated and tested for their effect on the dynamics. As shown in Figs. 10(a)–(d) the ADP-G-actin sequestering activity of twinfilin was the only one that leads to a biphasic evolution, qualitatively similar to the dynamics manifested when the full activity of twinfilin is simulated. Fig. 10(a) shows the evolution of the filament length distribution in the presence of 1.7 μM of twinfilin, whereas Fig. 10(b) shows the evolution of the length distribution in the presence of 1.7 μM of an ADP-G-actin sequestering protein with the same sequestering kinetics as twinfilin, but with no capping activity. The simulation predicts that the emergence of a biphasic growth evolution persists in the absence of the capping activity. Fig. 10(c) shows the evolution of the length distribution in the presence of 1.7 μM of a capping protein with the same capping kinetics as twinfilin, but with no monomer sequestering activity. It is evident that the capping activity in the absence of monomer sequestration fails to induce biphasic dynamics. The same is true in Fig. 10(d), which focuses on a generic monomer sequestering protein that exhibits no preferential binding to either ADP-G-actin or ATP-G-actin. These experiments, in conjunction with the experiments in Figs. 8(a)–(d), indicate that although other biochemical pathways presumably do exist in the growth assays of Helfer et al. (2006), it is the ADP-G-actin sequestering activity of twinfilin that drives the system towards extensive depolymerization after the establishment of an ADP-G-actin pool.

4. Discussion

The importance of the nucleotide composition of actin filaments in the regulation of filament dynamics by actin-accessory proteins is well documented in the experimental literature (Pollard and Borisy, 2003). However, a computational analysis of the evolution of nucleotide compositions and the resulting feedback to actin-binding proteins has been attempted in the theoretical literature only under severe modeling restrictions. These include restrictions on the properties of the filament length distribution (Bindschadler et al., 2004) and restrictions on the dynamic evolution of the monomer pool and the F-actin ATP hydrolysis pathway (Stukalin and Kolomeisky, 2006, among others). The necessity for such simplifications appears due to the computational and analytic complexity of investigating the dynamics of the filament length distribution *in conjunction* with the nucleotide compositions. Recent attempts to simulate the compound dynamics (Fass et al., 2007) are based on reducing the computational burden by artificially maintaining a small aggregate of filaments in the implementation of the simulation algorithm.

In this article, we developed an efficient Gillespie-type algorithm for generating numerical realizations of the master equation describing the reaction network of actin and actin-accessory proteins. The optimization of the computational cost of the method was based on the specific structure of the network under consideration. This

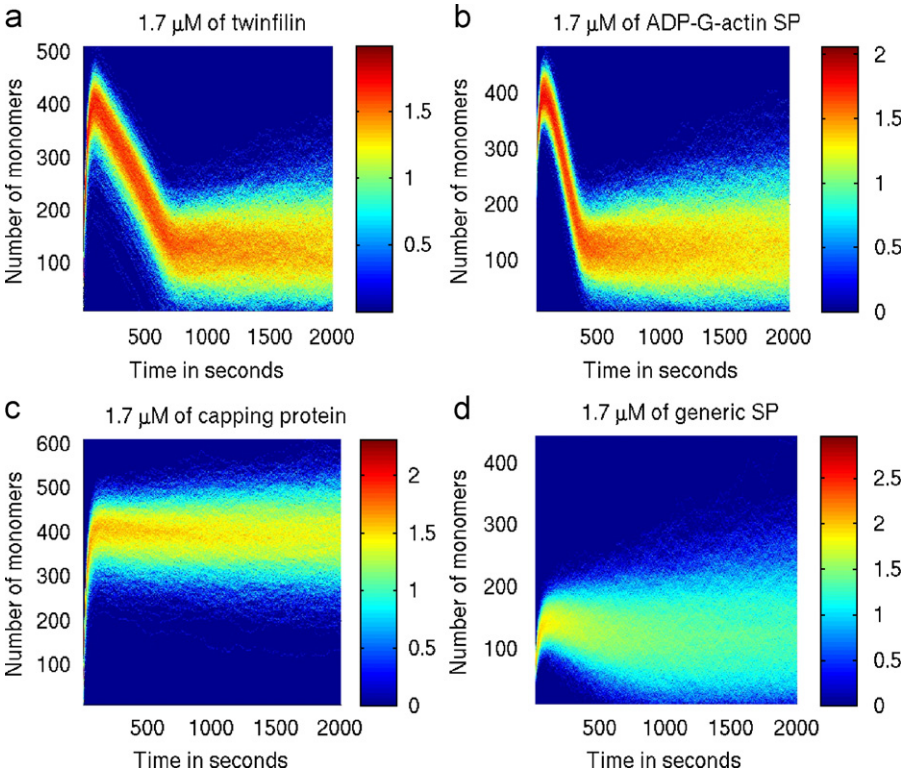

Fig. 10. Evolution in time of the filament length distribution (a) in the presence of 1.7 μM of twinfilin, (b) in the presence of 1.7 μM of a generic ADP-G-actin sequestering protein (SP) with no capping activity, (c) in the presence of 1.7 μM of a generic capping protein with no monomer sequestering activity and (d) in the presence of 1.7 μM of a generic sequestering protein with no nucleotide-binding specificity. The color code is on a logarithmic scale.

is in a different direction from that followed in relevant research work focusing on optimizing Gillespie's method (Gibson and Bruck, 2000; Cao et al., 2004; E et al., 2005), where the interest is on general reaction networks and no attempt is made to take advantage of the specific network topology.

To better understand how our method differs from these approaches we briefly discuss the current state of research in optimizing Gillespie's direct and first reaction methods for arbitrary reaction networks.[4] Gibson and Bruck (2000) focus on the first reaction method, and improve it in terms of computational cost by organizing the two data sets that contribute to the complexity of the method according to appropriate data structures. A *dependency graph* enables the algorithm to update only the relevant reaction rates, when an update due to the occurrence of a reaction is required. Moreover, an *indexed priority queue* is used to order the putative times at which the various reactions occur. A characteristic of the latter scheme is that, in the presence of n reactions it requires only $\mathcal{O}(\ln n)$ operations to re-organize the data structure, as opposed to $\mathcal{O}(n)$ operations for re-organizing a linear ordering. This approach has led Gibson and Bruck (2000) to an efficient formulation of the first reaction method, called the next reaction method.

Although the next reaction method significantly improves on the performance of the first reaction method, recent work by Cao et al. (2004) disputes the claim made by Gibson and Bruck (2000) that it is also more efficient than Gillespie's direct method. They provide evidence from profiling implementations of the next reaction method and the direct method, according to which for realistic network topologies the maintenance of the data structures used in the former becomes extremely costly in comparison to the performance of the latter.

As demonstrated here, the direct method is suboptimal for the reaction network consisting of actin and actin-accessory proteins. The efficiency of our method is crucial for simulating biologically realistic experiments, and having an efficient algorithm enabled us to analyze the experimental data of Helfer et al. (2006) on the capping and G-actin sequestering activity of twinfilin. In particular, we have shown that the biphasic evolution of the filament length distribution is the result of the ADP-G-actin sequestering activity of twinfilin, and that neither the capping activity of twinfilin nor the possible filament fragmentation activity due to the presence of gelsolin in the medium is required for the observed dynamics. We also provided evidence for the role of twinfilin in controlling the average filament length after a short burst of polymerization. Interestingly, our simulations indicate that the widely

[4]We refer the reader to Gillespie (2007) for a general discussion on the conceptual and computational differences between Gillespie-type algorithms and molecular dynamics simulations.

used pyrenyl-actin fluorescence experiments would fail to report the emergence of large filaments under certain experimental conditions.

References

Bindschadler, M., Osborn, E., Dewey, C., McGrath, J., 2004. A mechanistic model of the actin cycle. Biophys. J. 86, 2720–2739.

Blanchoin, L., Pollard, T., 2002. Hydrolysis of ATP by polymerized actin depends on the bound divalent cation but not profilin. Biochemistry 41, 597–602.

Cao, Y., Li, H., Petzold, L., 2004. Efficient formulation of the stochastic simulation algorithm for chemically reacting systems. J. Chem. Phys. 121 (9), 4059–4067.

E, W., Liu, D., Vanden-Eijnden, E., 2005. Nested stochastic simulation algorithm for chemical kinetic systems with disparate rates. J. Chem. Phys. 123, 194107.

Falck, S., Paavilainen, V., Wear, M., Grossmann, J., Cooper, J., Lappalainen, P., 2004. Biological role and structural mechanism of twinfilin–capping protein interaction. EMBO J. 23, 3010–3019.

Fass, J., Pak, C., Bamburg, J., Mogilner, A., 2007. Stochastic simulation of actin dynamics reveals the role of annealing and fragmentation. Biophys. J., submitted for publication.

Fujiwara, I., Vavylonis, D., Pollard, T., 2007. Polymerization kinetics of ADP- and ADP-Pi-actin determined by fluorescence microscopy. Proc. Natl Acad. Sci. 104 (21), 8827–8832.

Gadgil, C., Lee, C., Othmer, H., 2005. A stochastic analysis of first-order reaction networks. Bull. Math. Biol. 67, 901–946.

Gardiner, C., 1985. Handbook of Stochastic Methods for Physics, Chemistry and the Natural Sciences, second ed. Springer, Berlin.

Gibson, M., Bruck, J., 2000. Efficient exact stochastic simulation of chemical systems with many species and many channels. J. Phys. Chem. A 104, 1876–1889.

Gillespie, D., 1976. A general method for numerically simulating the stochastic time evolution of coupled chemical reactions. J. Comput. Phys. 22, 403–434.

Gillespie, D., 2007. Stochastic simulation of chemical kinetics. Annu. Rev. Phys. Chem. 58, 35–55.

Helfer, E., Nevalainen, E., Naumanen, P., Romero, S., Didry, D., Pantaloni, D., Lappalainen, P., Carlier, M.-F., 2006. Mammalian twinfilin sequesters ADP-G-actin and caps filament barbed ends: implications in motility. EMBO J. 25, 1184–1195.

Hu, J., Matzavinos, A., Othmer, H., 2007. A theoretical approach to actin filament dynamics. J. Stat. Phys. 128, 111–138.

Kuhn, J., Pollard, T., 2005. Real-time measurements of actin filament polymerization by total internal reflection fluorescence microscopy. Biophys. J. 88, 1387–1402.

Moseley, J., Okada, K., Balcer, H., Kovar, D., Pollard, T., Goode, B., 2006. Twinfilin is an actin-filament-severing protein and promotes rapid turnover of actin structures in vivo. J. Cell Sci. 119, 1547–1557.

Ojala, P., Paavilainen, V., Vartiainen, M., Tume, R., Weeds, A.G., Lappalainen, P., 2002. The two ADF-H domains of twinfilin play functionally distinct roles in interactions with actin monomers. Mol. Biol. Cell 13, 3811–3821.

Paavilainen, V., Bertling, E., Falck, S., Lappalainen, P., 2004. Regulation of cytoskeletal dynamics by actin-monomer-binding proteins. Trends Cell Biol. 14 (7), 386–394.

Pollard, T., Borisy, G., 2003. Cellular motility driven by assembly and disassembly of actin filaments. Cell 112, 453–465.

Selden, L., Kinosian, H., Estes, J., Gershman, L., 1999. Impact of profilin on actin-bound nucleotide exchange and actin polymerization dynamics. Biochemistry 38, 2769–2778.

Sept, D., Xu, J., Pollard, T., McCammon, J., 1999. Annealing accounts for the length of actin filaments formed by spontaneous polymerization. Biophys. J. 77, 2911–2919.

Stukalin, E., Kolomeisky, A., 2006. ATP hydrolysis stimulates large length fluctuations in single actin filaments. Biophys. J. 90, 2673–2685.